Joint Centre for Mesoscale Meteorology, Reading, UK

Consequences of the geostrophic momentum approximation on barotropic instability

A. J. Thorpe
S. Malardel
A. Joly

Internal Report No. 62

June 1996

Met Office Joint Centre for Mesoscale Meteorology Department of Meteorology
University of Reading PO Box 243 Reading RG6 6BB United Kingdom
Tel: +44 (0)118 931 8425 Fax: +44 (0)118 931 8791
www.metoffice.com

Designed and produced by the Met Office © Crown copyright 2001 01/0240 The Met Office logo is a registered trademark.

Consequences of the geostrophic momentum approximation on barotropic instability.

S.Malardel*, A.J.Thorpe+, A.Joly*

* : METEO-FRANCE, France,
+ : University of Reading, UK.

June 1996

Abstract

A subsynoptic instability with dominant barotropic signature has been found to be a possible mechanism for the development of frontal waves. Linear semi-geostrophic calculations of the growth rate of waves developing along a front exhibiting a low level potential vorticity band are here compared with the results of similar experiments made with a primitive equation model. The growth rates of the subsynoptic instability are significantly underestimated by the semi-geostrophic system, a result which is the opposite of what has been found by previous semi-geostrophic /primitive equation comparisons in the case of baroclinic instability calculations.

Analytical solutions of the Rayleigh model of pure barotropic instability confirm this behaviour of the geostrophic momentum approximation (GMA) in the case of barotropic instability. The inaccuracy of the equations with GMA is very sensitive to the basic wind shear amplitude. Such sensitivity seems to be directly linked with the definition of the semi-geostrophic vorticity.

It should be noted however that the frontal wave instability is not filtered by the balanced system but rather it is described in a quantitatively inaccurate way.

1 Introduction

One of the key aspects for understanding the dynamics of the atmosphere is to study the relative importance of the contribution of each term in the Navier-Stokes equations. Scale analysis is generally the method used to estimate the relative magnitude of these contributions. In midlatitudes, the large scale equilibrium is mainly geostrophic so the quasi-geostrophic system offers a good tool to study the dynamics of planetary to synoptic scale systems.

However the description of fronts, defined as a quasi-discontinuity occuring in a finite time, is not possible without the key-mechanism of ageostrophic wind advection which is at the origin of a frontogenetic feed-back on the circulation. This necessary ingredient is present when the geostrophic momentum approximation (GMA) is made in the primitive equation (Hoskins and Bretherton, 1972, Hoskins, 1975). The resulting system, the semi-geostrophic equations, is still a balanced system and offers several advantages such as a simpler numerical method and an easier interpretation of the results. In particular, the existence of an invertibility principle allows an efficient use of potential vorticity which is not possible with the full set of equations.

During these last 20 years, frontogenesis studies made with a semi-geostrophic model have improved our understanding of frontogenesis mechanisms (Hoskins and West, 1979, Davies, Schär and Wernli, 1991, Schär and Wernli, 1993). For baroclinic cyclone development at synoptic scale, comparisons have been made between semi-geostrophic and primitive equation results. Snyder, Skamarock and Rotunno (1991) and Bannon (1989) found, for example, that the linear growth rates are overestimated by the semi-geostrophic system. In nonlinear simulations, the differences between the semi-geostrophic and primitive equation results are amplified. The inaccurate behaviour of the semi-geostrophic equations in this case comes mainly from the semi-geostrophic vorticity equation whose ageostrophic contribution in the stretching term has the wrong sign (Snyder, Skamarock and Rotunno, 1991).

In this paper, a comparison between linear semi-geostrophic and primitive equation results is made. But the phenomena of interest are not the fronts

themselves but frontal waves, i.e. undulations occuring along extended trailing fronts at the end of the life cycle of the primary cyclone.

One of the possible explanations for the appearance of such waves was presented in Joly and Thorpe (1990, referred to below as JT90). Thus, the existence of a potential vorticity anomaly in a shear front may be at the origin of a mesoscale instability (wavelengths between 1800 and 800 km). The development of such an instability was latter simulated by a nonlinear primitive equation model (Malardel et al, 1993). It was found to be of a non-developmental type because the pressure deepening rates and wind increases induced by these perturbations are very modest, unless they are able to interact baroclinically. They however reorganize the circulation around a secondary minimum of pressure in a significant manner.

One of the main characterictics of these waves is their dominant barotropic signature. At least in the first stage of the development they grow mainly because of the kinetic energy of the front. Only the perturbation with the largest wavelengths (near the 1800 km bound) shows a second phase of growth with a baroclinic mechanism. Our aim in this paper is to assess the accuracy of the GMA in describing sub-synoptic scale instability which is due mainly to barotropic processes.

In the next section the type of fronts studied by JT90 is briefly described. Then, the JT90 semi-geostrophic normal mode growth rates and structures are compared with the results of a similar analysis made with a primitive equation model. Section 3 throws light on the differences observed between the semi-geostrophic and the primitive equation results in the case of frontal waves through an analytical analysis of the Rayleigh model of barotropic instability with and without GMA. A parallel is also drawn with the consequence of making the GMA in the baroclinic case.

2 Linear stability analyses of moist fronts

In JT90, linear stability analyses of two-dimensional fronts resulting from moist semi-geostrophic simulations of Eady modes were presented. A low level potential vorticity anomaly resulting from the precipitation is associated with a large along front wind gradient (figure 1). It allows the existence of an along-front instability (Charney and Stern, 1962) which is different from classic baroclinic instability. The

scale of this instability is found to be in the subsynoptic scale range (wavelengths between 1800 and 800 km) and it is characterized by a dominant barotropic type of development (extraction of horizontal kinetic energy form the basic state).

The validity of the semi-geostrophic system for such linear stability analyses at this scale may be queried. But an estimation of the validity of the GMA in terms of the smallness of the Lagrangian Rossby number (Hoskins, 1975) is not obviously relevant in a linear context as the radius of curvature has no meaning in this case. However, intuitively it can be expected that when the scale of the perturbation decreases, the radius of curvature of the air parcel trajectory decreases too. So, the GMA may reach its limit of validity. It is the aim of this paper to study if the use of a semi-geostrophic system is valid for the study of frontal waves.

2.1 Semi-geostrophic and primitive equation growth rate curves.

The linear stability analyses presented in JT90 have been repeated with a primitive equation limited area model (see Malardel et al, 1993 for a brief description of the model). A comparison between the previously obtained semi-geostrophic and the current primitive equation growth rates will now be presented. The method to compute the normal modes is in both cases a power method using the convergence criteria proposed in Simmons and Hoskins (1976). However, the numerical structures of the semi-geostrophic and the primitive equation models are different. The former is in geostrophic space with the prognostic variables being the semi-geostrophic potential vorticity in the interior and the potential temperature at the boundaries and the latter is a classical hydrostatic primitive equation model. Both have a doubly periodic geometry allowing the computation of the derivatives in spectral space. A verification of the coherence of the results obtained by these two models was done through baroclinic instability calculations and comparisons with previous studies using completely different numerical models. The basic state chosen for this validation is the uniform potential vorticity jet flow described in Hoskins and West (1979). As in Bannon (1989) and Snyder et al (1991), the overestimation of the growth rates by the semi-geostrophic model is clearly found (figure 2). A loss of symmetry in the perturbation structure on each side of the initial jet is also

observed.

Figure 3 and figure 4 show the semi-geostrophic and primitive equation growth rate curves in the case of two shear fronts modified by condensation studied in detail in JT90 and Malardel et al (1993). The main difference between these two fronts is the width of the potential vorticity anomaly. Front 1 has a wider anomaly (about 330 km) associated with weaker precipitation. Front 2, however, corresponds to a narrower anomaly (about 150 km) which occured during intense precipitation. According to the invertibility principle, for the wider anomaly, the signal of the large potential vorticity maximum is better seen in the potential temperature field (more baroclinicity) whereas the narrow anomaly in Front 2 has a signature in the vorticity field.

The differences observed between the semi-geostrophic and the primitive equation growth rate curves for these two cases are similar. The main feature is a large underestimation of the sub-synoptic growth rates by the semi-geostrophic model. In the case of Front 1 , it is accompanied by a shift of the most unstable wavelength towards larger scales. However, it can be noted that in the synoptic part of the curves, a slight overestimation of the growth rates by the semi-geostrophic model is still found as in the case of baroclinic developments along a jet flow.

2.2 Structures and energy conversions

The linear growth of a normal mode perturbation depends on the ability of the mode to draw energy from the basic state. The rate of energy extraction is exactly twice the growth rate of the mode. On the other hand, the efficiency of a mode to draw energy depends on its horizontal and vertical structure and especially on its horizontal and vertical tilts against the wind shear. The baroclinic conversion ($\overline{PE}$ to PE') is proportional to the potential temperature gradient and the potential temperature transport in the across front direction. The barotropic conversion ($\overline{KE}$ to KE') depends mainly on the product of the across front wind gradient and the correlation $u'v'$. The internal conversion (positive if PE' to KE') is linked with the vertical transport of heat.

A comparison between the semi-geostrophic and the primitive equation energy conversions for two modes of Front 1 (for a wavelength of 1800 km and 1200 km) and

one mode of Front 2 (for a wavelength of 800 km) is shown in figure 5. In each case, the semi-geostrophic values correspond to an underestimation of the rate of increase of the kinetic energy of the perturbation. For Front 1 , the barotropic conversion is seriously underestimated. In the case of Front 2 , it is rather the internal conversion from the perturbation kinetic energy reservoir to the perturbation potential energy reservoir which is overestimated.

The differences between the semi-geostrophic and the primitive equation structure of a mode for a given wavelength increase when the scale of the mode decreases, i.e. when the barotropic mechanism becomes dominant. The horizontal and vertical tilts are nearly the same in both models but the shape of the fields, especially the *geostrophic* fields, is modified when the GMA is made. The error on the full wind mainly comes from a large error in the geostrophic part of the wind, in shape, and also in amplitude[1] (figure 6). It is this inaccuracy in the computation of the geostrophic structure which leads to the poor estimation of the barotropic conversion even if, for the smallest wavelengths, the amplitude of the ageostrophic wind has the same order of magnitude as the geostrophic wind.

The potential temperature which is also deduced from the geopotential field is strongly influenced by the GMA too. The quasi non-tilted structure of the potential temperature field (only a slight baroclinic tilt) which is characteristic of a barotropic type mode is not well captured by the semi-geostrophic model. In the case of the mode of Front 1 with a 1800 km wavelength, the semi-geostrophic tilt is favorable for baroclinic instability at low levels only. The tilt changes in the middle of the atmosphere. Thus, on average, the semi-geostrophic model slightly underestimates the baroclinic conversion. Nevertheless, the global primitive equation energy cycle is still more characteristic of a barotropic type mode because of its negative internal conversion (figure 7).

2.3 Summary

It is clear therefore that in contrast to the overestimation of the growth rates by the SG model for synoptic scale baroclinic instability the theory with GMA provides an underestimate of the growth rates associated with frontal waves which are of sub-

[1]Each mode is normalized by the maximum of its across front wind perturbation.

synoptic scale. This difference in behaviour is surprising and unexpected. To find the origin of these differences, in the next section we construct and solve the classical Rayleigh problem of barotropic instability comparing the primitive equations and the GMA equations. The motivation for doing this is to find the simplest problem which might reveal the origin of the underestimation in the growth rate by the GMA theory. The barotropic model is indeed simple and it seems to capture the essence of the frontal wave instability described herein. The barotropic problem is pursued in section 3.1 and 3.2. In section 3.2 the baroclinic instability problem is also discussed so as to clarify why the SG theory acts in a different way for those larger scales.

3 Analysis of the Rayleigh problem

3.1 Uniform shear flow model

The model described in this section is a simple example illustrating barotropic instability. It was first studied by Rayleigh (1880) and solved in a quasi-geostrophic context in Gill (1982). In its QG version, its mathematical resolution is very similar to the one of the Eady model (Eady, 1949). The problem is posed on a f-plane (O,x,y). The wind of the basic state is zonal and depends only on y, the meridional direction. It is defined in three zones :

$$\begin{cases} -L < y < L & \overline{U} = \Lambda y \\ y > L & \overline{U} = \Lambda L \\ y < -L & \overline{U} = -\Lambda L \end{cases}$$

Λ is the uniform horizontal shear in the central region and is taken to be negative corresponding to cyclonic relative vorticity in a frontal zone (figure 8).

With the quasi-geostrophic and the primitive equation systems, a necessary condition for barotropic instability on a f-plane is :

$$\int_{-y_{max}}^{y_{max}} A(\frac{d^2\overline{U}}{dy^2})c_i \; = \; 0 \qquad (1)$$

with A a constant and kc_i the growth rate of the wave of zonal wavenumber k. In the semi-geostrophic case, this condition may not be written in such a simple form because the advection of the geostrophic wind by the ageostrophic circulation involves both the geostrophic and the ageostrophic stream functions. However, in the Rayleigh problem where $d^2\overline{U}/dy^2 = 0$ everywhere except at two single points

where $y = \pm L$, the necessary condition for instability is satisfied for *each system* of equations.

In the following section, the problem of linear stability of this basic state is solved analytically in two different cases : barotropic non-divergent equations with and without making the geostrophic momentum approximation (GMA).

In each case, a dispersion relation which gives a relationship between the growth rate of the mode σ and its zonal wavelength results from analytical calculations. From this relation, the growth rate and the wavenumber (or wavelength) of the most unstable mode are computed and expressed in terms of the characteristics of the basic state. The aim of this study is mainly to compare these numbers in the two cases. Differences between the mode structures will also be discussed briefly.

3.2 Analytical solution

3.2.1 The basic equations

Here we give the primitive momentum equations decomposed into geostrophic and ageostrophic parts. The quasi-geostrophic system approximates the acceleration terms by using the geostrophic wind. As in the quasi-geostrophic system, the prognostic variable in the semi-geostrophic system is the geostrophic wind, but it is now advected by the full wind. Thus, the feed back of the ageostrophic circulation on the geostrophic flow is taken into account (derivation given in detail in Hoskins, 1975).

The resulting equations are then :

$$(\frac{\partial}{\partial t} + u\frac{\partial}{\partial x} + v\frac{\partial}{\partial y})(u_g + mu_a) - fv_a = 0 \tag{2}$$

$$(\frac{\partial}{\partial t} + u\frac{\partial}{\partial x} + v\frac{\partial}{\partial y})(v_g + mv_a) + fu_a = 0 \tag{3}$$

where $u = u_g + nu_a$, $v = v_g + nv_a$ and n and m are tracer parameters such that $m = n = 0$ gives the quasi-geostrophic case; $n = 1$ and $m = 0$ gives the semi-geostrophic case; and $m = n = 1$ gives the primitive equations. It turns out that as far as the growth rate equation is concerned the primitive equation case and the QG case are identical if in the QG case the geostrophic streamfunction is used, $\psi = \phi/f$. This is because both the geostrophic component and the ageostrophic component

are separately non-divergent and so their sum can be described by a streamfunction. In the derivation of the growth rate equation it does not matter whether we deal with the total streamfunction or the geostrophic streamfunction. Therefore in the derivation that follows we will set $m = 0$ without losing generality, i.e. with $n = 1$ then the GMA is made whilst if $n = 0$ the growth rate equation applies equally to QG or primitive equations. Note however that this similarity between the QG and the PE results from the non-divergent hypothesis. It disappears in cases where the flow is divergent. Thus, such similarity between the QG and the PE systems does not signify that the QG system is more general than the GMA one. In fact, in the non-divergent case, two approximations compensate in the QG vorticity equation to give a form similar to the non divergent PE vorticity equation which may be written as follows using the tracer parameters n and m defined above :

$$\left(\frac{\partial}{\partial t} + \overline{U}\frac{\partial}{\partial x}\right)\left(\zeta'_g + mn\zeta'_a\right) + \overline{\zeta}\left(m\frac{\partial u'_a}{\partial x} + n\frac{\partial v'_a}{\partial y}\right) + f\left(\frac{\partial u'_a}{\partial x} + \frac{\partial v'_a}{\partial y}\right) = 0$$

The term in ζ disappears in the PE case when the flow is non-divergent. This term does not exist at all in the QG case as both the ageostrophic advection and the Lagrangien evolution of the ageostrophic wind are neglected. But, in the GMA case, one half of this term remains as the advection of $\overline{U}$ by v'_a remains. The formal similarity between the PE and the QG systems is used here to provide a simple way to solve the PE problem.

It appears that the vorticity is not a conservative quantity when the GMA is made. However, a "semi-geostrophic" vorticity may be defined as in Hoskins (1975) :

$$\xi_{SG} = \frac{\partial v_g}{\partial x} - \frac{\partial u_g}{\partial y} + \frac{1}{f}\frac{\partial(u_g, v_g)}{\partial(x, y)}$$

ξ_{SG} is conserved by the semi-geostrophic barotropic system of equations. So,

$$\left(\frac{\partial}{\partial t} + u\frac{\partial}{\partial x} + v\frac{\partial}{\partial y}\right)\xi_{SG} = 0 \tag{4}$$

The system of equations (2) and (3) plus the continuity equation are linearized around the basic state defined in section 3.1. The flow is therefore divided into $(u_g, v_g) = (\overline{U} + u'_g, v'_g)$ and $(u_a, v_a) = (u'_a, v'_a)$ where prime indicates a small perturbation. In order to obtain the growth rate equation it is easiest to use these linearized equations and the geostrophic wind relationships $(u'_g, v'_g) =$

$1/f\left(-\frac{\partial\phi'}{\partial y}, \frac{\partial\phi'}{\partial x}\right)$. Substituting for v'_a from the linearized form of equation (2) into the linear vorticity equation gives the following basic equation determining the y-structure of ϕ':

$$\frac{\partial^2\phi'}{\partial y^2} + n\frac{\partial\phi'}{\partial y}\frac{\partial^2\overline{U}}{\partial y^2}\frac{1}{f\Delta^2} - \phi'\left(\frac{\partial^2\overline{U}}{\partial y^2}\frac{1}{\Delta^2(\overline{U}-c)} + k^2\Delta^2\right) = 0 \tag{5}$$

where

$$\Delta^2 = 1 - \frac{n}{f}\frac{\partial\overline{U}}{\partial y}$$

is a positive parameter for cyclonic basic state. If $n = 0$ then we obtain the classical Rayleigh equation for barotropic instability whereas $n = 1$ is for the GMA.

To solve this equation matching conditions at the edges of the vorticity strip have to be found. These are continuity of pressure or ϕ' and the second condition can be obtained by integrating equation (5) across the two strip edges. It can be shown that equation (5) can be written in the form:

$$\frac{\partial}{\partial y}\left(\frac{\partial\phi'}{\partial y}\frac{1}{\Delta^2}\right) - \phi'\left(\frac{f}{n(\overline{U}-c)}\frac{\partial}{\partial y}\left(\frac{1}{\Delta^2}\right) + k^2\right) = 0 \tag{6}$$

To find the second boundary condition we integrate across an edge of the vorticity strip, at Y $(= \pm L)$, from $(Y-\epsilon)$ to $(Y+\epsilon)$. Noting that ϕ' and $\overline{U}$ are continuous at the interface we obtain upon integration at the limit when ϵ tends towards zero :

$$\Delta^2\Big|_{(Y-\epsilon)}\frac{\partial\phi'}{\partial y}\Big|_{(Y+\epsilon)} - \Delta^2\Big|_{(Y+\epsilon)}\frac{\partial\phi'}{\partial y}\Big|_{(Y-\epsilon)} = \frac{\phi'\left(\frac{\partial\overline{U}}{\partial y}\Big|_{(Y+\epsilon)} - \frac{\partial\overline{U}}{\partial y}\Big|_{(Y-\epsilon)}\right)}{(\overline{U}-c)} \tag{7}$$

This condition must be applied at both edges of the vorticity strip along with continuity of ϕ'.

3.2.2 Solution

A solution which satisfies the basic equation (5) and the boundary conditions is :

$$\begin{cases} \phi'(x,y,t) = (a\ \sinh(\Delta ky) + b\ \cosh(\Delta ky))e^{ik(x-ct)} & |y| < L \\ \phi'(x,y,t) = A\ e^{-ky}\ e^{ik(x-ct)} & y > L \\ \phi'(x,y,t) = B\ e^{ky}\ e^{ik(x-ct)} & y < L \end{cases}$$

The dispersion relation is then given by:

$$\begin{aligned} -\sigma^2 &= \frac{\Lambda^2}{\Delta^2}\frac{[\ \Delta kL(\Delta\cosh(\Delta kL) + \sinh(\Delta kL)) - \cosh(\Delta kL)\ ]}{[(\cosh(\Delta kL) + \Delta\sinh(\Delta kL)]} \\ &\times \frac{[\ \Delta kL(\cosh(\Delta kL) + \Delta\sinh(\Delta kL)) - \sinh(\Delta kL)\ ]}{[\Delta\cosh(\Delta kL) + \sinh(\Delta kL)]} \end{aligned} \tag{8}$$

If $n = 0$ then $\Delta = 1$ and the expression reduces to the classical Rayleigh formula which is valid for both the quasi geostrophic and the primitive equation growth rate calculations. The most unstable mode has a wavenumber k_{max} such that $k_{max}L = 0.4$; it does not depend on the value of the shear. The maximum growth rate σ_{max} depends linearly on Λ : $\sigma_{max} = \sigma(k_{max}) = |\Lambda| * 0.2$ (figure 9, dashed-cross line).

With $n = 1$, the GMA case, the maximum growth rate σ_{max} is not a linear function of Λ as is the case for the classical Rayleigh problem. For different values of Λ, the growth rate curves giving σ/Λ as a function of kL are shown in figure 9 (solid lines). The value of σ_{max} is underestimated in the Rayleigh barotropic model when the GMA is made and the error increases quickly when the horizontal shear Λ increases. On the other hand, the wavelength of the most unstable mode is shifted towards larger scales in the results with GMA ; this shift is amplified when the shear increases. Thus, in this simple model of pure barotropic instability, the growth rates of the normal modes have a similar behaviour when the GMA is made as in the study of the JT90 basic states.

The structures of the normal mode solutions are also sensitive to the GMA. As for the growth rates, the error of the semi-geostrophic model increases quickly when the shear of the basic state increases. Figure 10 shows a comparison between the solutions found for u'_g by the primitive equation and the semi-geostrophic versions of the Rayleigh problem for $\Lambda = -2f$, a length $L = 10^5 \mathrm{s}^{-1}$ and a wavenumber $k = 2.10^{-6}\mathrm{m}^{-1}$. A qualitative comparison may be made with the results of the wind structure shown in figure 6. The semi-geostrophic model has two maxima on each side of the zone where the wind changes sign instead of one maximum in the middle of the domain found in the primitive equation case. On the other hand, for the shear front modes, the ageostrophic wind structure is rather less inaccurate than the geostrophic one (figure 11).

It is also interesting to note that the Rayleigh problem with GMA may be solved in geostrophic space. However, the Jacobian term in the expression for the SG vorticity

$$J' = \frac{1}{f} \frac{\partial \overline{U}}{\partial y} \frac{\partial v'_g}{\partial x}$$

(Hoskins, 1975) is not negligible in this case and so the SG solution in geostrophic space is not exactly similar to the QG problem (and in the non-divergent case, to the PE problem). But the results obtained if J' is neglected have the same type of errors (when compared with the PE results) as the GMA results with J' included. It is illuminating to interpret the results if we take $J' = 0$. In this case, the SG growth rate and unstable wavenumbers are obtained from the PE ones with a very simple scaling

$$\sigma_{SG} = \frac{1}{\Delta^2}\sigma_{PE}$$
$$k_{SG} = \frac{1}{\Delta^2}k_{PE}$$

due to the change of shear and geometry in the geostrophic space. In a cyclonic zone, Δ^2 is larger than 1 which corresponds to the underestimation of the growth rates and the shift towards the larger scales by the SG system.

An other way to interpret physically this rescalling is to consider barotropic instability as the result of Rossby edge wave interaction in an horizontal plane. Thus, in geostrophic space, the distance between the interacting Rossby waves is $L^* - \Delta^2 L$ because of the stretching in the cyclonic zone. The interaction between both waves is then less efficient and, in consequence, the growth rate is smaller. On the other hand, the effective scale of the wave in the Y-direction is proportional to $1/k$. Thus, the edges of the domain are farther apart in geostrophic space, which explains that instabilities occur for larger scales.

At this stage, it is possible to interpret the different behaviour of GMA in the case of barotropic instability and in the case of baroclinic instability (section 2.1). In a classic three-dimensional description of baroclinic instability, the vertical shear and the vertical distance between the top and the bottom of the domain where the Rossby edge waves propagate are not modified by the coordinate transformation if the basic state is independent of the zonal coordinate. However, the vertical gradient of temperature is smaller in geostrophic space :

$$\underbrace{\frac{\partial\overline{\theta}}{\partial Z}}_{>0} = \underbrace{\frac{\partial\overline{\theta}}{\partial z}}_{>0} + \underbrace{f\frac{\partial\overline{U}}{\partial z}\frac{\partial\overline{\theta}}{\partial Y}}_{<0}$$

Thus, the Rossby wave depth which is proportional to $1/N$ is larger in geostrophic space than in physical space. Then the Rossby edge waves interact more efficiently

which corresponds to the overestimation of the growth rates and the shift of the wavenumber cut-off towards the smaller scales in the case of baroclinic instability. This is the opposite effect compared to that obtained for barotropic instability.

In conclusion, the GMA has to be used carefully to solve barotropic type instability. The validity of the GMA depends on a Rossby number. An estimation of the ratio between inertia term and Coriolis term which in the Rayleigh model may be written

$$r_o = \frac{\left|(\frac{\partial}{\partial t} + \overline{U}\frac{\partial}{\partial x})u'\right|}{|fv'|} = \frac{|\Lambda|Lk}{f}$$

is always smaller than 1.4 for wavenumbers in the range of instability. Such values are easily accepted in baroclinic studies. Thus, it has been shown here that the Rayleigh barotropic instability is well posed when the GMA is made but the detailed solution of the problem with GMA shows non-negligible errors in the growth rates and structures even for reasonable shears.

4 Conclusions

The GMA applied to the non-divergent barotropic equation modifies the results of the Rayleigh model. The growth rate curve for this pure barotropic instability still shows a maximum of instability, but the maximum growth rate is underestimated and the most unstable wave number is shifted toward larger scales. This inaccuracy of the GMA increases quickly as the constant shear Λ of the basic wind becomes larger. These results account for what was found in section 2.1 in the case of the JT90 moist shear fronts, Front 1 and Front 2 (figures 3 and 4) which show a barotropic horizontal wind shear in the frontal region near the surface. As the subsynoptic modes have a strong barotropic component, the results of section 3.2 would explain such a departure between the semi-geostrophic and the primitive equation modes. On the other hand, the study of the Rayleigh model confirms that the differences between the primitive equation and the semi-geostrophic calculations result rather from a problem in the computation of the geostrophic part of the circulation although intuitively the ageostrophic part of the circulation might have been suspected.

In the Rayleigh model, the classic condition for barotropic instability (equation (1)) is satisfied by both the semi-geostrophic and the primitive equation

models. Thus, there is no instability of a type that the Charney and Stern theorem (1962) does not predict. However, semi-geostrophic results may be quantitatively quite inexact when the field structures are badly approximated.

Thus, as is true for any approximation, the GMA has some limitations in its precision which are reached in the case of perturbations mainly growing because of the horizontal wind shear of the basic state. The inaccuracy of the GMA for barotropic-type instability would probably also be amplified in the nonlinear evolution of the modes when the ageostrophic effects act fully, such as has been found in the baroclinic case (Snyder et al, 1991).

Aknowledgments : The authors would like to thank Chris Snyder for helpful comments about the role of the GMA, and Rich Rotunno for suggesting a simplification in our way of posing the Rayleigh problem.

References

P.R. Bannon, *Linear baroclinic instability with the geostrophic momentum approximation.*, J. Atmos. Sci. **46** (1989), 402–409.

J.G. Charney and M.E. Stern, *On the stability of internal baroclinic jets in a rotating atmosphere.*, J. Atmos. Sci. **19** (1962), 159–162.

H.C. Davies, Ch. Schär, and H. Wernli, *The palette of fronts and cyclones within a baroclinic wave development*, J. Atmos. Sci. **48** (1991), no. 14, 1666–1689.

E.T. Eady, *Long-waves and cyclone waves.*, Tellus **1** (1949), no. 3, 33–52.

A.E. Gill, *Atmosphere ocean dynamics.*, vol. 30, Academic Press, 1982, 662 pp, International geophysics series.

B.J. Hoskins, *The geostrophic momentum approximation and the semi-geostrophic equations.*, J. Atmos. Sci. **32** (1975), 233–242.

B.J. Hoskins and F.P. Bretherton, *Atmospheric frontogenesis models : mathematical formulation and solution.*, J. Atmos. Sci. **29** (1972), 11 37.

B.J. Hoskins and N.V. West, *Baroclinic waves and frontogenesis. part II: Uniform potential vorticity jet flows - cold and warm fronts.*, J. Atmos. Sci. **36** (1979), 1663–1680.

A. Joly, *Les processus diabatiques et la condensation de l'eau dans les fronts atmosphériques : application à l'étude de leur formation et de leur stabilité.*, Ph.D. thesis, Thèse de Doctorat de l'Université Paris VI, Paris, mars 1989, 470pp.

A. Joly and A.J. Thorpe, *Frontal instability generated by tropospheric potential vorticity anomalies.*, Quart. J. Roy. Meteor. Soc. **116** (1990), 525–560.

S. Malardel, A. Joly, F. Courbet, and Ph. Courtier, *Non-linear evolution of ordinary frontal waves induced by low-level potential vorticity anomalies*, Quart. J. Roy. Meteor. Soc. **119** (1993), 681 713.

Lord Rayleigh, *On the stability, or instability, of certain fluid motions.*, Proc. Lond. Math. Soc. **11** (1880), 57–70.

C. Schär and H. Wernli, *Structure and evolution of an isolated semi-geostrophic cyclone*, Quart. J. Roy. Meteor. Soc. **119** (1993), 57 -90.

A.J. Simmons and B.J. Hoskins, *Baroclinic instability on the sphere : normal modes of the primitive and quasi-geostrophic equations.*, J. Atmos. Sci. **33** (1976), 1454–1477.

C. Snyder, W.C. Skamarock, and R. Rotunno, *A comparison of primitive-equation and semi-geostrophic simulations of baroclinic waves*, J. Atmos. Sci. **48** (1991), no. 19, 2179–2194.

Figure captions :

Figure 1 : Horizontal across front sections of Front 1 from A.Joly, 1989. The across front wavelength is 3250km. The total height is 8km.

(a) Semi-geostrophic potential vorticity in physical space. ΔPV = 0.2pvu, reference 0.3pvu. The dashed-dotted contour is 0.2pvu, the dashed contour 0.4pvu.

(b) Along front wind. Contour every 5m.s^{-1} (solid lines). Potential temperature $\overline{\theta}$. $\Delta\theta = 4$K (dashed lines).

(c) Non dimensional absolute vorticity $\overline{J} - \overline{\zeta}_a/f$ (solid lines). $\Delta\overline{J} - 0.5f$. Reference f. Absolute momentum m (dashed lines). $\Delta m = 70$m.s^{-1}.

Figure 2 : Growth rates as a function of the along front wavenumbers of the normal modes computed with the HW79 jet flow as a basic state by the power method. The semi-geostrophic results from the JT90 model are dashed, the solid line corresponds to the computation of the primitive equation model.

Figure 3 : Growth rates as a function of the along front wavenumber in the case of Front 1.

Dashed curve : semi-geostrophic results

Solid curve : primitive equation results

Figure 4 : As in figure 3 but for Front 2 .

Figure 5 : Energy cycles for the 1800 km and 1200 km modes of Front 1 and the 800 km mode of Front 2 . PE and $\overline{KE}$ are the potential and kinetic energy reservoirs of the front, PE' and KE' are the reservoirs for the perturbation. Numbers in a box are the primitive equation results.

Figure 6 : Horizontal section of the along front wind perturbation at 950hpa for the 800 km mode of Front 2.

Primitive equation results on the left.

Semi-geostrophic results on the right.

Contours every 2 cm.s^{-1}. The across front wavelength is 3250km in both cases (only 1/3 is shown), the along front wavelength is 800km.

Figure 7 : Along front vertical cross section of θ' (section A-A of figure 1) for the 1800 km mode of Front 1.

Primitive equation results at the top.

Semi-geostrophic results at the bottom.

$\Delta\theta' = 0.03$K. The along front wavelength is 1800 km, the total height 8km.

Figure 8 : Wind profils of the Rayleigh model basic state for $\Lambda < 0$.

Figure 9 : σ/Λ as a function of kL for the calculation without GMA (solid line) or with GMA. The smallest curve corresponds to $\Lambda = -4f$ and then the next three ones are for $\Lambda = -3f$, $-2f$ and $-f$. In the case without GMA, the results are independant of Λ. In all cases, $L = 10^5$m.

Figure 10 : Structure of u'_g (to be compared with the along front wind perturbation of figure 6) for the Rayleigh mode with a wavenumber of 2.10^{-6}m^{-1}. In this case, the basic state is characterized by a length $L = 10^5$m and a shear $\Lambda = 2f$.

Primitive equation results on the top, semi-geostrophic results on the bottom. The x-direction corresponds with the along front direction of Front 1 or Front 2 (figure 6), the y-direction with the across front direction.

Figure 11 : Same as figure 10 but for u'_a.

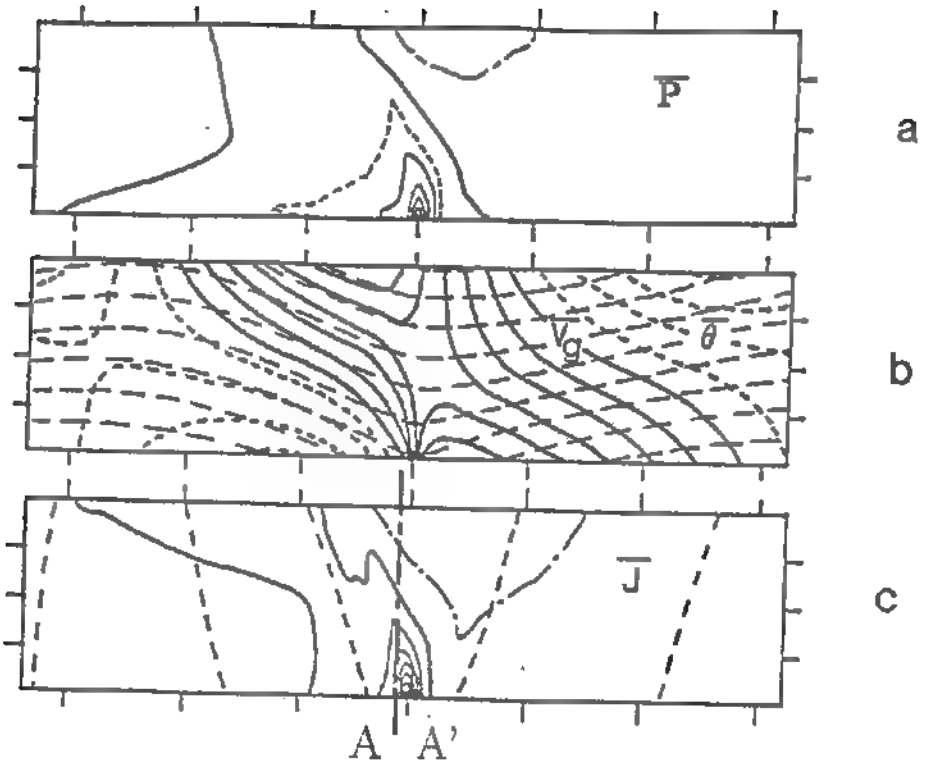

Figure 1:

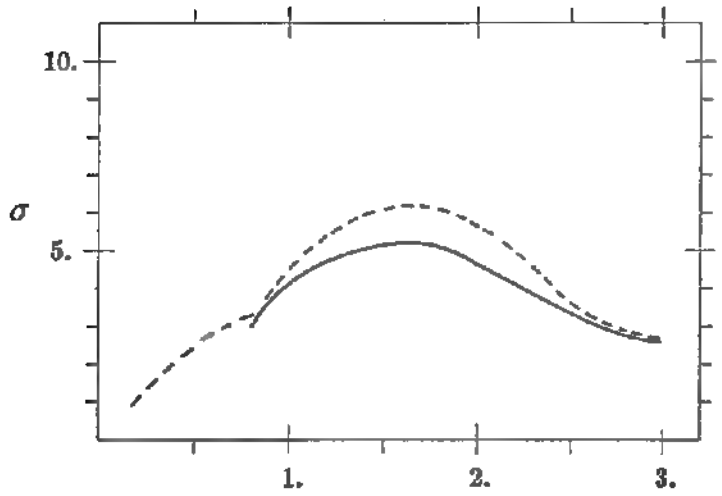

Figure 2:

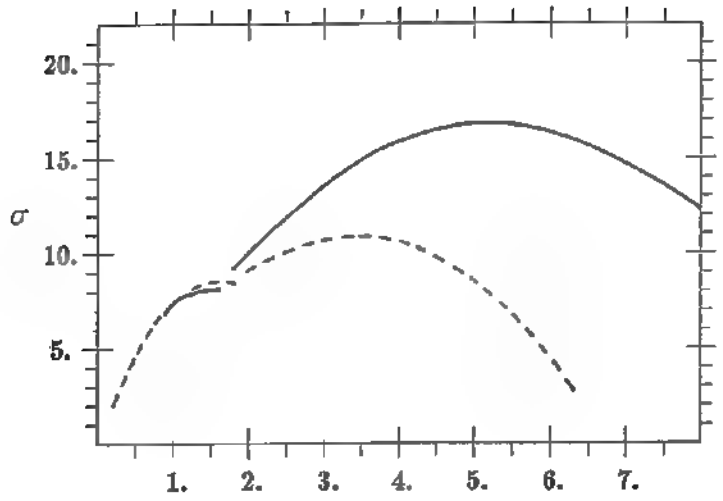

Figure 3:

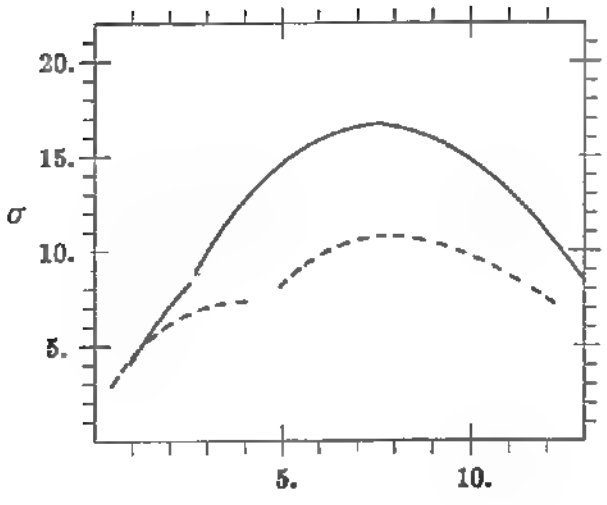

Figure 4:

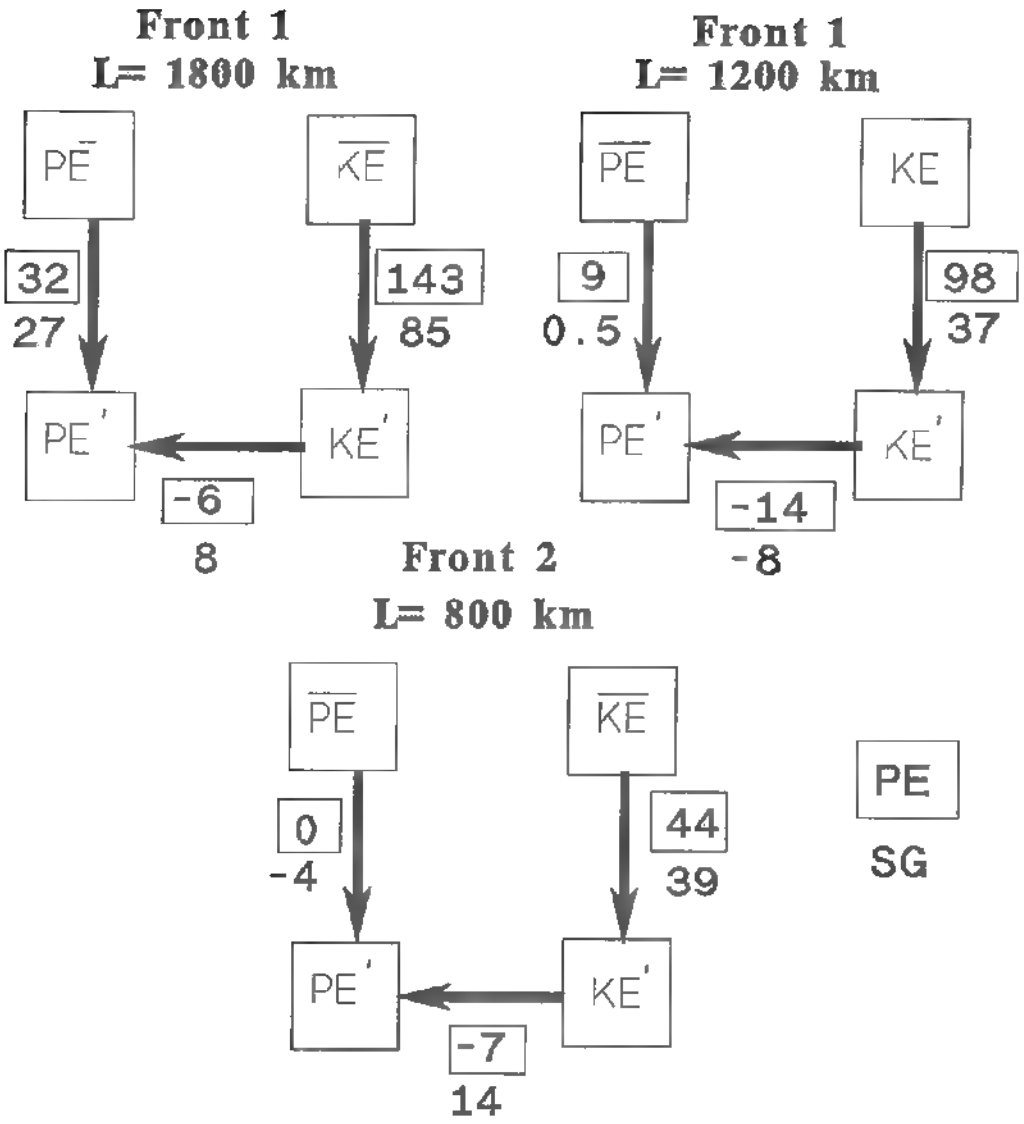
Front 1
L= 1800 km
PE
KE
32
27
143
85
PE'
KE'
-6
8
Front 1
L= 1200 km
PE
KE
9
0.5
98
37
PE'
KE'
-14
-8
Front 2
L= 800 km
PE
KE
0
-4
44
39
PE'
KE'
-7
14
PE
SG

Figure 5:

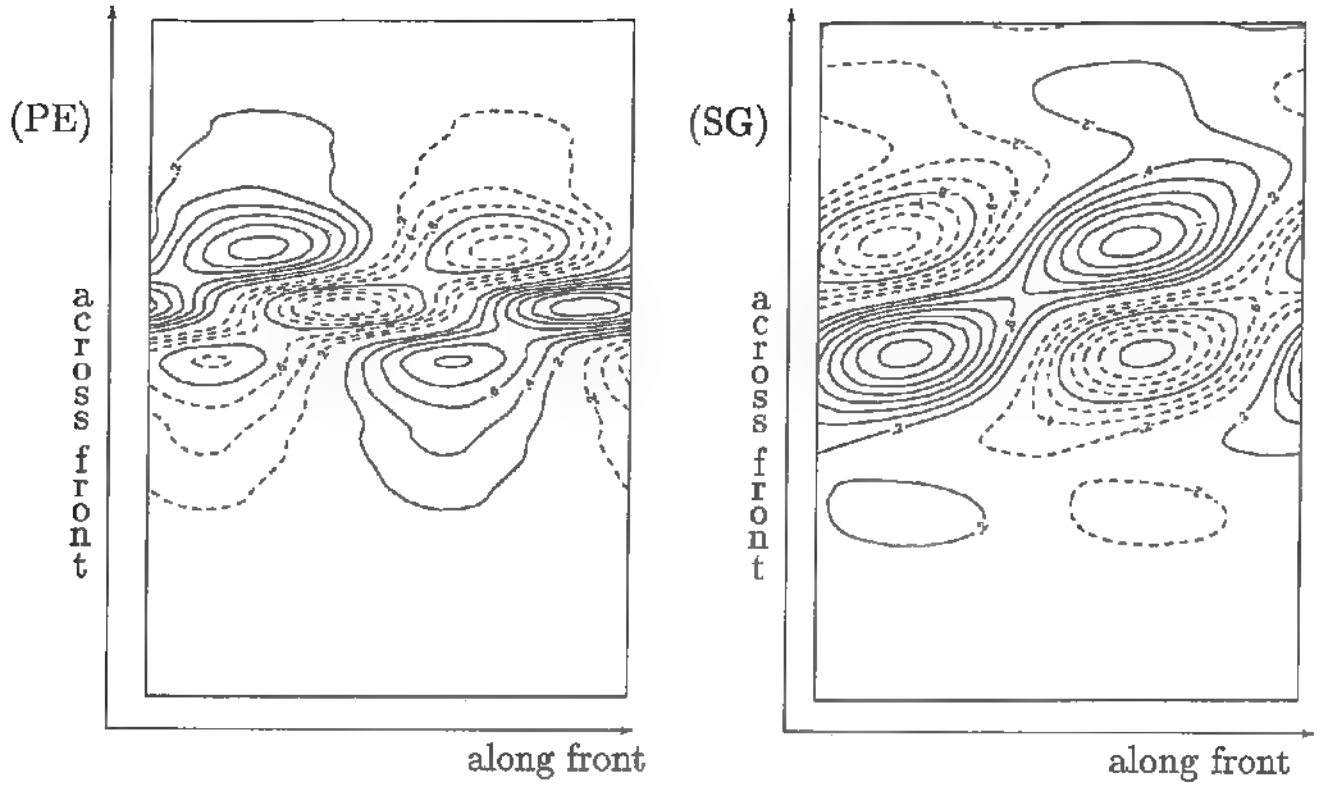

Figure 6:

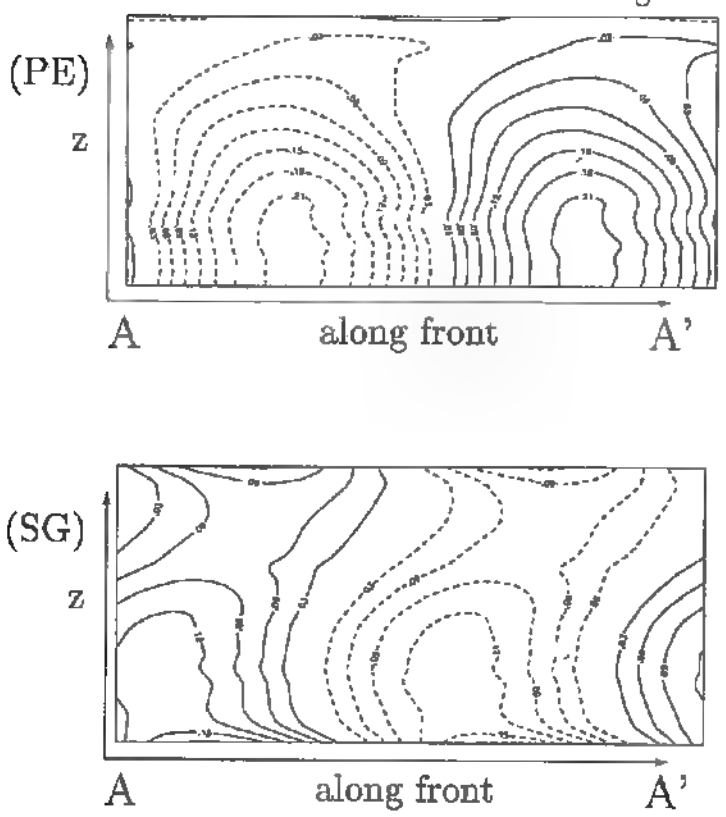

Figure 7:

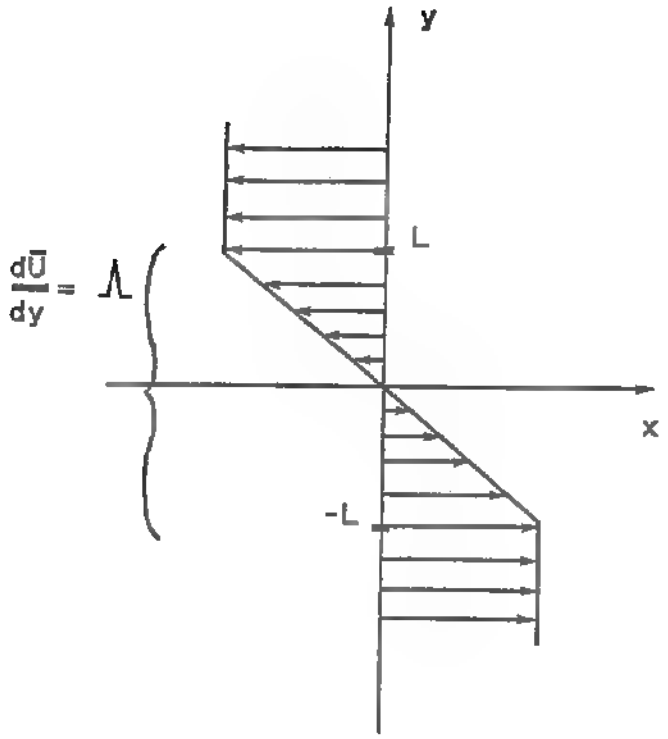

Figure 8:

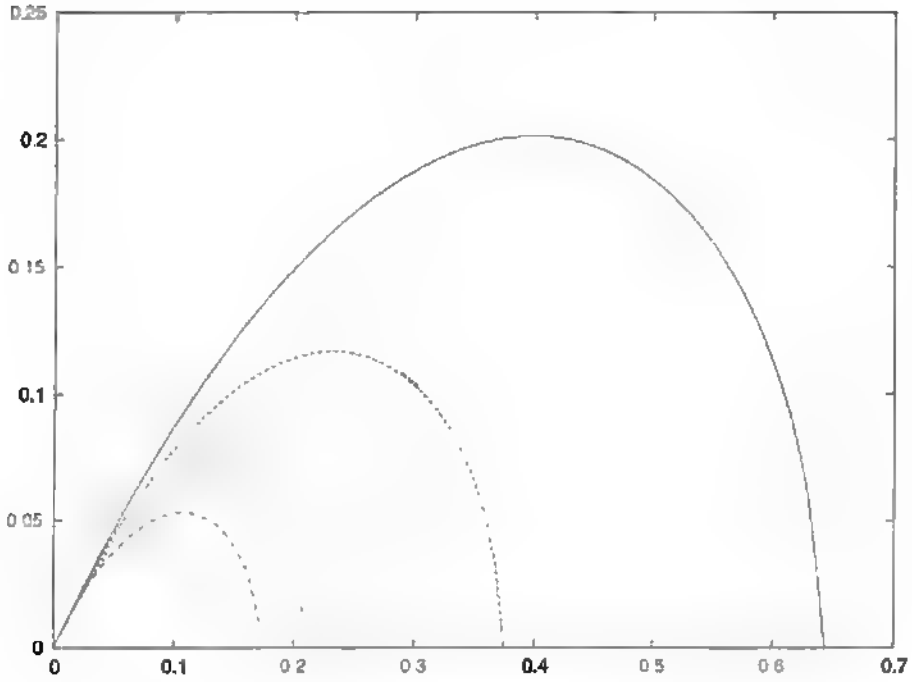

Figure 9:

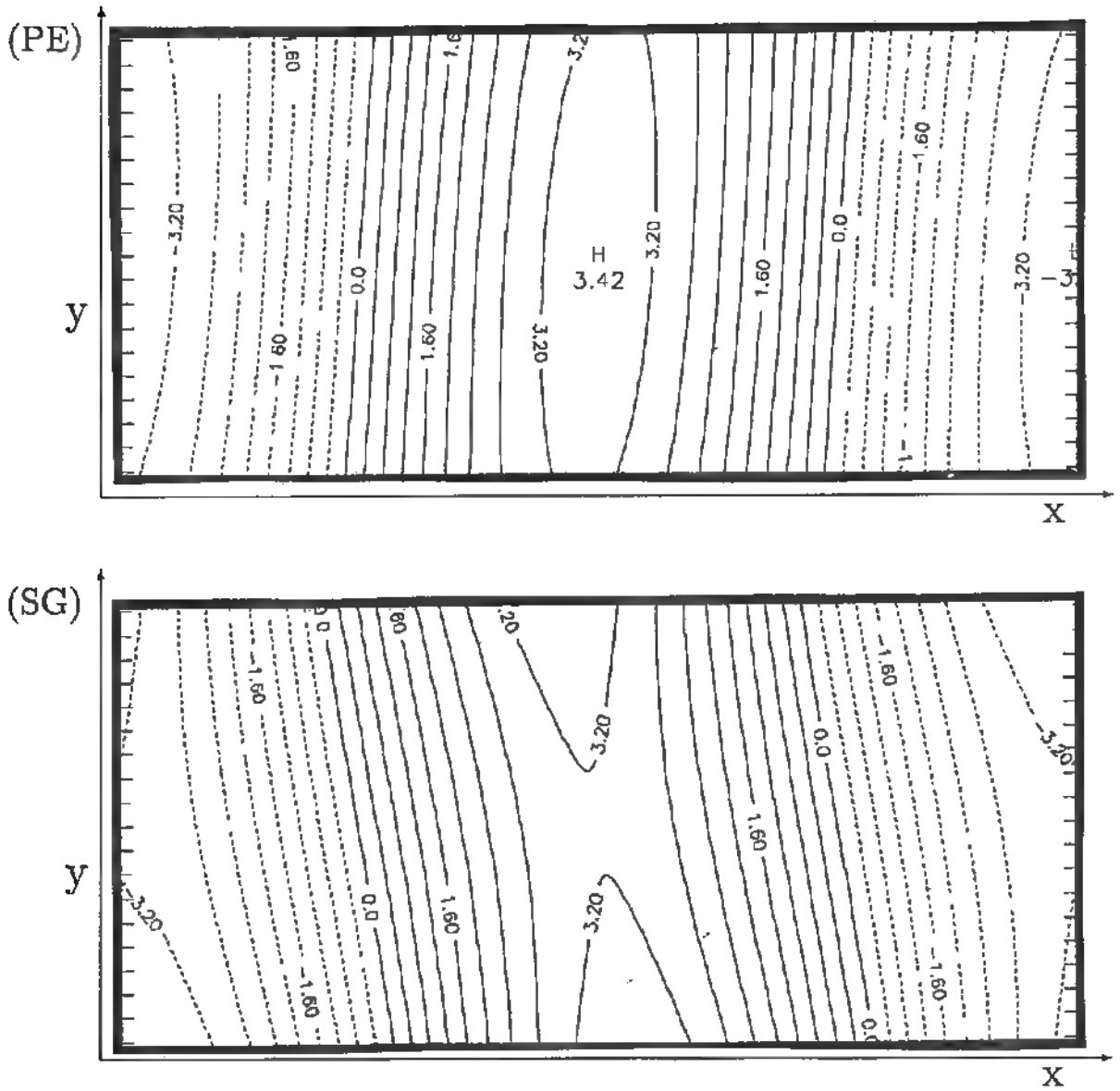

Figure 10:

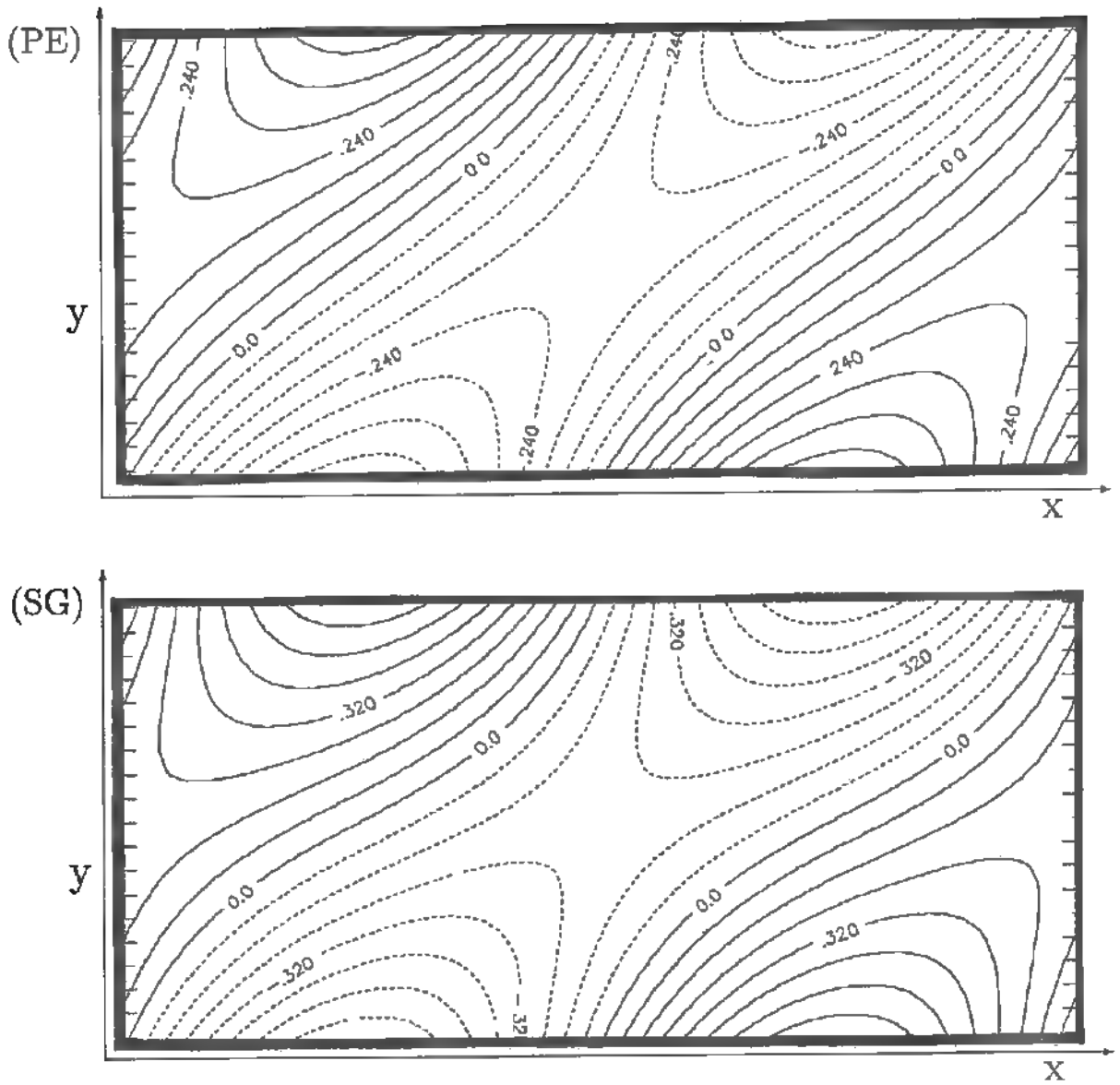

Figure 11:

CURRENT JCMM INTERNAL REPORTS

This series of JCMM Internal Reports, initiated in 1993, contains unpublished reports and also versions of articles submitted for publication. The complete set of Internal Reports is available from the National Meteorology Library on loan, if required.

1. **Research Strategy and Programme.**
   K A Browning et al
   January 1993

2. **The GEWEX Cloud System Study (GCSS).**
   GEWEX Cloud System Science Team
   January 1993

3. **Evolution of a mesoscale upper tropospheric vorticity maximum and comma cloud from a cloud-free two-dimensional potential vorticity anomaly.**
   K A Browning
   January 1993

4. **The Global Energy and Water Cycle**
   K A Browning
   July 1993

5. **Structure of a midlatitude cyclone before occlusion.**
   K A Browning and N Roberts
   July 1993

6. **Developments in Systems and Tools for Weather Forecasting.**
   K A Browning and G Szejwach
   July 1993

7. **Diagnostic study of a narrow cold frontal rainband and severe winds associated with a stratospheric intrusion.**
   K A Browning and R Reynolds
   August 1993

8. **Survey of perceived priority issues in the parametrizations of cloud-related processes in GCMs.**
   K A Browning
   September 1993

9. **The Effect of Rain on Longwave Radiation.**
   I Dharssi
   September 1993

10. **Cloud Microphysical Processes - A Description of the Parametrization used in the Large Eddy Model.**
H Swann
July 1994

11. **An Appreciation of the Meteorological Research of Ernst Kleinschmidt.**
A J Thorpe
May 1992

12. **Potential Vorticity of Flow Along the Alps.**
A J Thorpe, H Volkert and Dietrich Heimann
August 1992

13. **The Representation of Fronts.**
A J Thorpe
January 1993

14. **A Parametrization Scheme for Symmetric Instability: Tests for an Idealised Flow.**
C S Chan and A J Thorpe
February 1993

15. **The Fronts 92 Experiment: a Quicklook Atlas.**
Edited by T D Hewson
November 1993

16. **Frontal wave stability during moist deformation frontogenesis. Part 1. Linear wave dynamics**
C H Bishop and A J Thorpe
May 1993

17. **Frontal wave stability during moist deformation frontogenesis. Part 2. The suppression of non-linear wave development.**
C H Bishop and A J Thorpe
May 1993

18. **Gravity waves in sheared ducts.**
S Monserrat and A J Thorpe
October 1993

19. **Potential Vorticity and the Electrostatics Analogy: Quasi-Geostrophic Theory.**
C Bishop and A J Thorpe
November 1993

20. **Recent Advances in the Measurement of Precipitation by Radar.**
A J Illingworth
April 1993

21. **Micro-Physique et Givrage. Cloud Microphysics and Aircraft Icing.**
A J Illingworth
May 1993

22. **Differential Phase Measurements of Precipitation.**
M Blackman and A J Illingworth
May 1993

23. **Estimation of Effective Radius of Cloud Particles from the Radar Reflectivity.**
N I Fox and A J Illingworth
May 1993

24. **A Simple Method of Dopplerising a Pulsed Magnetron Radar.**
L Hua, A J Illingworth and J Eastment
November 1993

25. **Radiation and Polar Lows.**
George C Craig
February 1994

26. **Collected preprints submitted to International Symposium on the Life Cycles of Extratropical Cyclones; Bergen, Norway, 27 June - 1 July 1994**
April 1994

27. **Convective Frontogenesis**
Douglas J Parker and Alan J Thorpe
April 1994

28. **Improved Measurement Of The Ice Water Content In Cirrus Using A Total Water Evaporator**
Philip R A Brown and Peter N Francis
April 1994

29. **Mesoscale Effects of a Dry Intrusion within a Vigorous Cyclone**
K A Browning and B W Golding
April 1994

30. **GEWEX Cloud System Study, Science Plan**
May 1994

31. **Parametrization of Momentum Transport by Convectively Generated Gravity Waves**
R Kershaw
February 1995

32. **Mesoscale Modelling Newsletter, No. 5**
May 1994

33. **Observations of the mesoscale sub-structure in the cold air of a developing frontal cyclone**
K A Browning, S A Clough, C S A Davitt, N M Roberts and T D Hewson
May 1994

34. **Longwave Radiative Forcing of a Simulated Tropical Squall Line**
Imtiaz Dharssi
July 1994

35. **On the nature of the convective circulations at a kata-cold front**
K A Browning
September 1994

36. **Collected preprints of papers submitted to the COST-75 International Seminar on Advanced Weather Radar Systems, Brussels, 20-23 September 1994**
November 1994

37. **Use of satellite imagery to diagnose events leading to frontal thunderstorms: Parts I and II of a case study**
K A Browning and N M Roberts
November 1994

38. **The role of spaceborne millimetre-wave radar in the global monitoring of ice cloud**
P R A Brown, A J Illingworth, A J Heymsfield, G M McFarquhar, K A Browning and M Gosset
December 1994

39. **Potential Vorticity Inversion**
Michal Ziemianski
October 1994

40. **Theory of mature tropical cyclones; A comparison between Kleinschmidt (1951) and Emanual (1986)**
Suzanne L Gray
December 1994

41. **Dispersion and removal of pollutants during the passage of an atmospheric frontal system**
N R Gimson
December 1994

42. **The role of snow sublimation in frontogenesis**
D J Parker and A J Thorpe
December 1994

43. **Potential vorticity and the electrostatics Analogy: Ertel-Rossby formulation**
A J Thorpe and C H Bishop
December 1994

44. **Mesoscale aspects of extratropical cyclones: an observational perspective**
K A Browning
January 1995

45. **A Polar Low Outbreak: Evolution and Mesoscale Structures**
T D Hewson, G C Craig and C Claud
February 1995

46. **Generation of near-surface gusts by deep convection**
K Nakamura and R Kershaw
April 1995

47. **Attribution concepts applied to the omega equation**
S A Clough, C S A Davitt and A J Thorpe
June 1995

48 **Parametrization of mixed-phase cloud and precipitation**
Susan P Ballard and M Gerard Hutchinson
June 1995

49 **Short-range forecasting of stratocumulus: Initialization V Prediction**
Susan P Ballard, Simon D Jackson and B Macpherson
June 1995

50 **Contributions of the JCMM/Dept of Meteorology Radar Group to the 27th AMS Radar Meteorology Conference, Vail October 1995**
June 1995

51 **Cold pools in shear**
Douglas J Parker
September 1995

52 **High-resolution analysis of frontal fracture**
K A Browning, S P Ballard and C S A Davitt
September 1995

53 **The Albedo of Broken Cloud Fields: Calculations using a modified two stream radiation code**
Imtiaz Dharssi and Roy Kershaw
October 1995

54 **Parametrization of momentum transport by convection. I: Theory and cloud modelling results**
R Kershaw and D Gregory
November 1995

55 **Variation of frontal structure along a cold front**
K A Browning and N M Roberts
November 1995

56 **Secondary Frontal Waves**
Douglas Parker
December 1995

57 **Objective Fronts**
T D Hewson
March 1996

58 **Mesoscale analysis of the activation of a cold front during cyclogenesis**
K A Browning, N M Roberts and A J Illingworth
June 1996

59 **Investigation of different representations of rain in a 1-d evaporation model**
H Swann
May 1996

60 **Parametrization of diabatic processes in the inversion of the omega-equation**
M Athanassiadou and A J Thorpe

61 **The role of the environmental flow in the development of secondary frontal cyclones**
I A Renfrew, A J Thorpe and C H Bishop

62 **Consequences of the geostrophic momentum approximation on barotropic instability**
S Malardel, A J Thorpe and A Joly
June 1996

Met Office Joint Centre for Mesoscale Meteorology Department of Meteorology
University of Reading PO Box 243 Reading RG6 6BB United Kingdom
Tel: +44 (0)118 931 8425 Fax: +44 (0)118 931 8791
www.metoffice.com